

Temperature-dependent scattering rate and optical mass of ferromagnetic metallic manganites

J. R. Simpson, H. D. Drew, V. N. Smolyaninova, R. L. Greene, M. C. Robson, Amlan Biswas, and M. Rajeswari
Center for Superconductivity Research, Department of Physics, University of Maryland, College Park, Maryland 20742

(Received 1 September 1999)

We report on the optical properties of the hole-doped manganites $\text{La}_{0.7}\text{Ca}_{0.3}\text{MnO}_3$ and $\text{La}_{0.7}\text{Sr}_{0.3}\text{MnO}_3$. Transmission and reflection of thin films are measured in the infrared at temperatures from 10 to 150 K using Fourier-transform spectroscopy. The scattering rate and optical mass are obtained by fitting the far-infrared transmission data to a Drude model. The scattering rate shows a T^2 dependence with temperature. The optical mass enhancement differs only slightly from specific heat results. In addition, we compare the infrared spectral weight to band-structure calculations. [S0163-1829(99)52144-9]

The recent discovery of colossal magnetoresistance (CMR) in hole-doped manganites of the form $\text{La}_{1-x}\text{A}_x\text{MnO}_3$ where La is a lanthanide and A is an alkaline-earth element has renewed interest in this complex magnetic system. For doping concentrations in the range $0.2 < x < 0.5$, this material undergoes a phase transition from paramagnetic insulator to ferromagnetic metal at the Curie temperature T_c . The double-exchange model (DE) first proposed by Zener¹ explains the phase transition in terms of the Mn d electrons, namely, the strong Hund's coupling between the three electrons localized in the t_{2g} orbitals and the $1-x$ electrons in the e_g orbitals. While DE qualitatively describes the metal-insulator transition at T_c , recent experimental²⁻⁴ and theoretical⁵ work indicates the importance of coupling between charge and the lattice, specifically the dynamic Jahn-Teller (JT) effect. Below T_c , itinerant conduction results from ferromagnetic ordering increasing the width of the e_g band and suppressing the JT effect. Evidence for charge and orbital ordering at different doping concentrations suggests the ground state may be the result of competition between interactions with the lattice and different types of ordering: ferromagnetic, charge, and orbital. At present, the exact nature of the low-temperature state is not fully understood.

Optical conductivity studies^{2,3,6-9} have shown a shift in spectral weight from the visible to the infrared as the temperature is lowered below T_c . In the ferromagnetic state, the low-frequency optical spectrum is characterized by Drude-like conduction. Several groups have reported an anomalously small Drude weight in both $\text{La}_{0.7}\text{Ca}_{0.3}\text{MnO}_3$ (LCMO) and $\text{La}_{0.7}\text{Sr}_{0.3}\text{MnO}_3$ (LSMO).⁶⁻⁸ Interpreting the small Drude weight in terms of an enhanced optical mass, the effective mass values reported in these optical studies are much greater than the results from specific heat measurements.^{10,11} Small apparent Drude weight may also be understood in terms of charge ordering. A charge density wave opens a partial gap in the density of states at the Fermi level $N(E_f)$, increasing the optical mass while decreasing the specific heat mass. However, recent findings have cast doubts on these small Drude weights.^{9,12}

In this paper, we concentrate on the optical conductivity, scattering rate, and mass enhancement of thin-film manganites at temperatures below T_c . At these temperatures, the low-frequency conductivity exhibits a Drude-like behavior. We find an optical mass which is comparable to the specific

heat mass, a result which is inconsistent with strong charge ordering in these optimally doped materials. The results suggest that the metallic state of the ferromagnetic manganites is a Fermi liquid.

Thin films of LCMO and LSMO are grown on LaAlO_3 (LAO) substrates using pulsed laser deposition. The LCMO film was subsequently annealed in an O_2 environment.¹³ Low residual resistivity $\rho(T=4\text{ K})$, and high resistivity peak temperature T_p indicate the excellent quality of the films. For LCMO, $\rho(T=4\text{ K})=124\ \mu\Omega\text{ cm}$ and $T_p=275\text{ K}$, and for LSMO, $\rho(T=4\text{ K})=15\ \mu\Omega\text{ cm}$ and $T_p>350\text{ K}$.

Transmittance $\mathcal{T}(\omega)$ and reflectance $\mathcal{R}(\omega)$ measurements of near-normal incidence light are performed using a Fourier-transform spectrometer.² Temperature-dependent spectra from 10 to 150 K ($T < T_c$) are obtained. We focus on two frequency ranges: the far-infrared (far-IR) 2.5–15 meV and the midinfrared (mid-IR) 0.2–1.2 eV. The spectral gap between 15 and 200 meV is due to the opacity of LAO in this spectral range. Determination of the film conductivity in both frequency ranges requires knowledge of the index of refraction n and extinction coefficient of the substrate, which is measured separately.

In the far-IR, the thin-film transmittance (transmission of the film/substrate divided by transmission of the bare substrate) is given by

$$\mathcal{T}(\omega) \approx \frac{1}{|1 + Z(\omega)\sigma(\omega)|^2}; \quad Z(\omega) = \frac{Z_0 d_f}{n(\omega) + 1}, \quad (1)$$

where Z_0 is the impedance of free space, d_f is the film thickness, and $\sigma(\omega)$ is the complex optical conductivity. [Note that while not explicitly expressed in Eq. (1), multiple reflections are included in the analysis.]

Given the Drude-like low-frequency behavior of the conductivity below T_c observed in these materials,^{2,6,9} we fit the measured \mathcal{T} with a simple Drude model

$$\sigma(\omega) = \frac{1}{4\pi} \frac{\omega_p^{*2}}{\gamma^* + i\omega}, \quad (2)$$

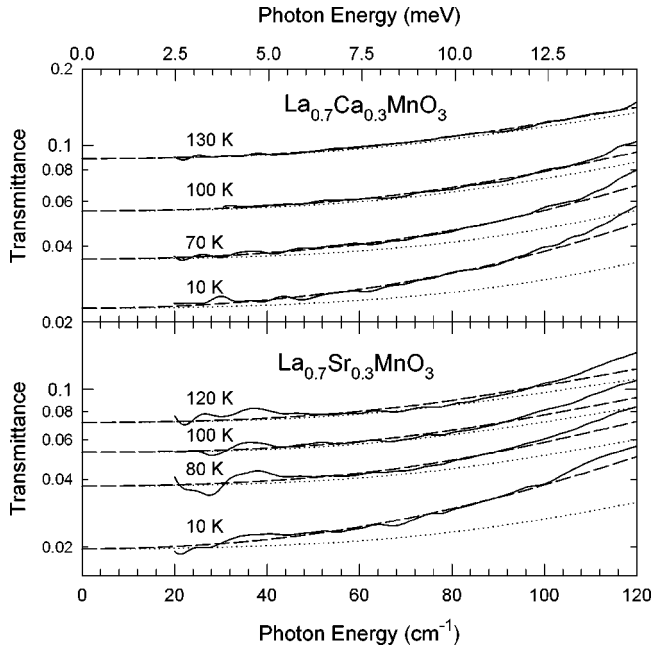


FIG. 1. Transmittance of LCMO and LSMO as a function of photon energy for several temperatures. Solid lines are data, dashed lines are fits to a simple Drude model, and dotted lines are Drude fits in the limit, $\gamma^* \rightarrow \infty$.

where γ^* is the effective scattering rate and ω_p^* is the effective plasma frequency or spectral weight of the Drude conductivity.

Transmittance curves in the far-IR (solid lines) and fits to a Drude model (dashed lines) for several temperatures are shown in Fig. 1. The low-frequency T increases with temperature corresponding to a decrease in the conductivity. At higher temperatures, T deviates less from the limiting value (dotted lines) where $\gamma^* \rightarrow \infty$. In the infinite scattering-rate limit, $\sigma(\omega) \rightarrow \sigma_0$ and therefore the frequency dependence of the limiting case is due to the $n(\omega)$ of the LAO substrate. The slight upturn of the data relative to the fit curves (dashed lines) above 100 cm^{-1} appears independent of temperature (note that uncertainty in T increases as the frequency nears the substrate cutoff around 120 cm^{-1}).

Fitting the measured T with Eq. (2), we show the temperature dependence of the resulting γ^* and ω_p^* in Fig. 2. The scattering rate has a T^2 temperature dependence and is fit (solid line) with $\gamma^*(T) = \gamma_0^* + (k_B T)^2/W$, where the fitting parameters are the defect scattering rate at zero temperature γ_0^* and the characteristic energy for inelastic scattering W , and k_B is Boltzmann's constant. W values for LCMO and LSMO are listed in Table I. As temperature increases, T approaches the limiting value and the uncertainty in determining both γ^* and ω_p^* increases. Figure 2 shows error bars for γ^* in (a) and ω_p^* in (b). γ^* falls below the T^2 fit at the highest temperatures (140 and 150 K for LCMO and 150 K for LSMO). At this time, we are uncertain as to the cause of this apparent decrease in the scattering rate and whether it continues above 150 K. While γ^* exhibits a strong temperature dependence, ω_p^* remains relatively independent of temperature.

Having obtained γ^* and ω_p^* , we determine the zero-frequency resistivity

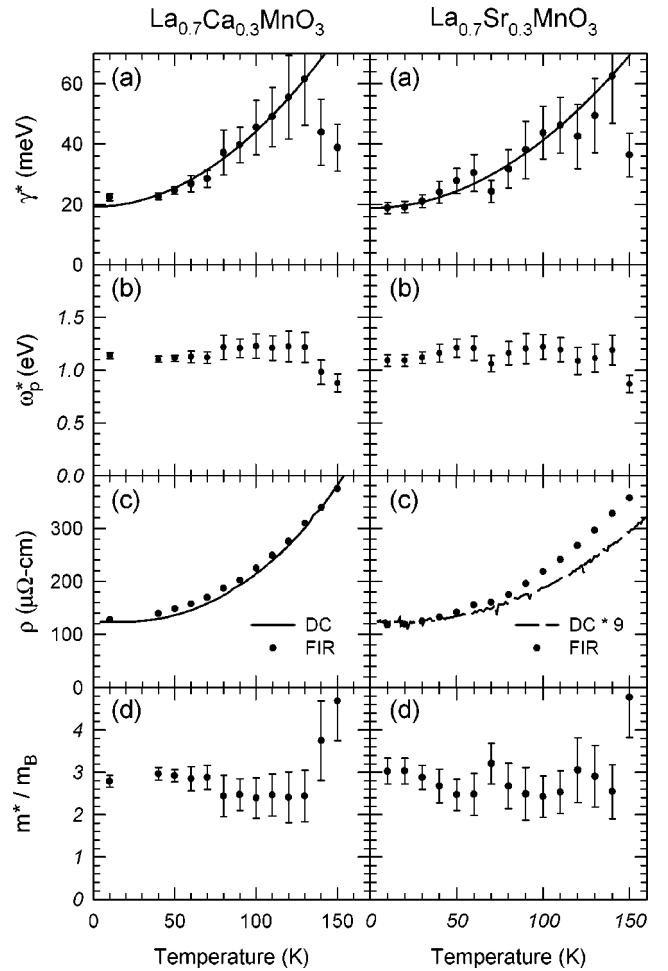


FIG. 2. Temperature dependence of the scattering rate γ^* (a), plasma frequency ω_p^* (b), resistivity ρ (c), and mass enhancement m^*/m_B (d) obtained from fitting the far-IR transmittance using a Drude conductivity. γ^* is fit (solid line) to T^2 . The dc resistivity in (c) is plotted for comparison (note for LSMO the dc resistivity is multiplied by a factor of 9). Error bars are shown explicitly in (a), (b), and (d) and are nominally the size of the solid circles in (c).

$$\rho = \frac{4\pi\gamma^*}{\omega_p^{*2}} = \frac{4\pi\gamma}{\omega_p^2}. \quad (3)$$

Temperature dependence of ρ is shown in Fig. 2(c). Both the far-IR values (solid circles) derived from Eq. (3) and the dc values (lines) from standard four-probe measurements are plotted for comparison. dc and far-IR resistivity agree reasonably well in LCMO, however, the dc value for LSMO has been scaled by a factor of 9. Similar results for LSMO films were reported earlier² and attributed to an anisotropic con-

TABLE I. Mass enhancements from optics ($T=10 \text{ K}$) and specific heat and characteristic scattering-rate energies.

Sample	m^*/m_B			
	Optics	Specific heat ^a	W (meV)	ω_0 (meV)
LCMO	2.8 ± 0.2	4.05 ± 0.09	3.0	≤ 76
LSMO	3.0 ± 0.3	3.06 ± 0.14	3.3	≤ 87

^aReference 10.

ductivity resulting from substrate induced strain. Uncertainty in the far-IR ρ (error bars are nominally the size of the points) results from uncertainty in the film thickness and detector noise.

The optical mass enhancement is defined by

$$m^*/m_B = (\omega_p^B/\omega_p^*)^2 = 1 + \lambda, \quad (4)$$

where λ is the mass enhancement factor and the plasma frequencies, ω_p^B and ω_p^* , are obtained from band-structure calculations and far-IR measurements, respectively. Pickett and Singh¹⁶ predict $\omega_p^B = 1.9$ eV for LCMO. A tight-binding parametrization of the band structure with hopping parameter, $t_0 = 0.6$ eV, gives $\omega_p^B = 2.1$ eV.² Taking $\omega_p^B = 1.9$ eV, mass enhancement as a function of temperature is shown in Fig. 2(d) and found to be approximately 3 for both materials.

The T^2 temperature dependence of γ^* suggests that γ^* may also be frequency dependent. The analysis presented above assumed a frequency independent γ^* and ω_p^* . A modification to the Drude theory is necessary to consider a frequency dependent γ^* . To obtain an optical conductivity that is a proper response function satisfying Kramers-Kronig relations, a frequency-dependent scattering rate must include a real and imaginary part, $\gamma(\omega) = \gamma_1(\omega) + i\gamma_2(\omega)$, where $\gamma_2(\omega) = \omega\lambda(\omega)$. This leads to the extended Drude model¹⁷ with a renormalized scattering rate, $\gamma^* = \gamma/(1 + \lambda(\omega))$, and a renormalized plasma frequency, $\omega_p^* = \omega_p/\sqrt{1 + \lambda(\omega)}$. Thus, the frequency-dependent scattering gives rise to a concomitant frequency-dependent mass enhancement, $m^*/m_B(\omega) = 1 + \lambda(\omega)$.

In order to obtain $m^*/m_B(\omega)$ for these transmission measurements, we must assume (since we cannot measure directly) a form for the frequency dependence of γ . The T^2 dependence of γ^* implies a similar ω^2 dependence at low frequency.¹⁸ This gives the full temperature- and frequency-dependent scattering rate, $\gamma^*(\omega, T) \propto \omega^2 + (p\pi T)^2$. Gurzhi calculated $p = 2$ for electron-electron scattering.¹⁹ For heavy fermion systems, Sulewski *et al.*¹⁸ found that the experimental data was consistent with $p \leq 1$. They proposed a simple phenomenological model, $\gamma(\omega) = \gamma_0 + \lambda_0\omega\omega_0/(\omega - i\omega_0)$, which satisfies the ω^2 behavior at low frequencies and saturates at a characteristic frequency ω_0 . Using W from the T^2 fits to γ^* (see Fig. 2) and a value for p , ω_0 may be determined. Taking $p = 1$, we find less than a 15% effect on the mass enhancement and $\omega_0 \gg 15$ meV, the high-frequency cutoff of our far-IR measurements (ω_0 values for $p = 1$ are shown in Table I). Thus, in the far-IR, the frequency dependence of γ^* and m^*/m_B is not significant.

The T^2 dependence of γ^* and relative T independence of m^*/m_B differs with results reported on a LCMO polycrystalline sample.⁶ We believe that the discrepancy is due to the effects of surface damage introduced during the polishing of the bulk samples. Recently, Takenaka *et al.*¹² and Lee *et al.*⁹ discussed the importance of polishing and surface scattering effects in measuring bulk reflectivity for polycrystalline and single-crystal samples. They found the optical properties of these materials are sensitive to surface preparation. Specifically, polishing produced a decrease in mid-IR reflectivity and the apparent spectral weight. Cleaving or annealing the polished surfaces removes these effects, bringing the results on bulk samples in reasonable agreement with thin films.

It is interesting to compare the mass enhancement obtained from optical measurements reported here with specific heat results. The low-temperature ($3 < T < 8$ K) specific heat is $C_H = \gamma_{el}T + \delta T^{3/2} + \beta T^3$ where the three terms arise from charge carriers, magnons, and phonons, respectively.¹¹ The coefficient of the linear (electronic) term is $\gamma_{el} = \pi^2 k_B^2 N(E_f)/3 \propto m^*$. For LCMO and LSMO, γ_{el} is 4.5 ± 0.1 and 3.4 ± 0.15 mJ/mole K², respectively. Relating the experimental γ_{el} to band theory predictions gives the specific heat mass enhancement, $m^*/m_B = \gamma_{el}/\gamma_{el}^B = 1 + \lambda$, analogous to the optical enhancement in Eq. (4). Pickett and Singh¹⁶ predict $N(E_f) = 0.47$ states/eV for the majority spin band giving $\gamma_{el}^B = 1.1$ mJ/mole K². Mass enhancements calculated using this γ_{el}^B are shown in Table I. Including the $N(E_f)$ for the minority spin bands (smaller than majority by approximately a factor of 2) increases γ_{el}^B and ω_p^{B2} . This tends to reduce the specific heat mass enhancement while increasing the optical mass enhancement. However, minority carriers are expected to be localized by cation disorder¹⁶ and are not included in this report. A comparison of m^*/m_B from optics ($T = 10$ K) and specific heat as shown in Table I indicates reasonable agreement between the two values. This agreement contrasts with the earlier results on LCMO (Ref. 6) and LSMO (Refs. 7 and 8) bulk samples where large optical masses are reported. Thus, the agreement we find between the two mass enhancements suggests that charge ordering correlations are not strong in the CMR manganite alloys at $x = 0.3$ doping.

The strength of the inelastic scattering is large as is indicated by the small value of W in Table I: $W \ll E_f \approx 1$ eV. For electron-electron scattering, W is typically on the order of E_f . This is consistent with the relatively large mass enhancement in these materials in comparison with conventional metals. The value of the characteristic frequency ω_0 is in reasonable accord with the expectations of electron-phonon interaction where ω_0 would be somewhat larger than the average phonon frequency of the system. Explanations for the temperature dependence of the scattering rate include magnons²⁰ and phonons.²¹ However, the origin of the T^2 scattering is not currently understood.

In the mid-IR, the Fresnel \mathcal{T} and \mathcal{R} formulas for a film on an absorbing substrate¹⁴ are inverted numerically to obtain optical constants, such as $\sigma(\omega)$ or the dielectric constant $\epsilon(\omega)$, without the need for Kramers-Kronig analysis.¹⁵ Figure 3 shows the real part of the optical conductivity σ_1 and the real part of the dielectric constant ϵ_1 (inset) in the mid-IR for LCMO. The observed negative ϵ_1 is characteristic of a metal. For $T < 150$ K, σ_1 exhibits negligible temperature dependence and consequently we present only the $T = 10$ K data (solid line). In this spectral range, σ_1 increases at low frequency and eventually must extrapolate to the far-IR value (solid circle). For comparison, the Drude conductivity resulting from the fit parameters, γ^* and ω_p^* , is shown as a dotted line. The extrapolated conductivity associated with the Drude model is less than the observed mid-IR value.

While the mass enhancement analysis does not show an anomalously small Drude weight, it is interesting to compare the observed far-IR Drude weight with the total spectral weight from both mid-IR measurements and band-structure calculations. In order to compare these spectral weights, we introduce the kinetic energy

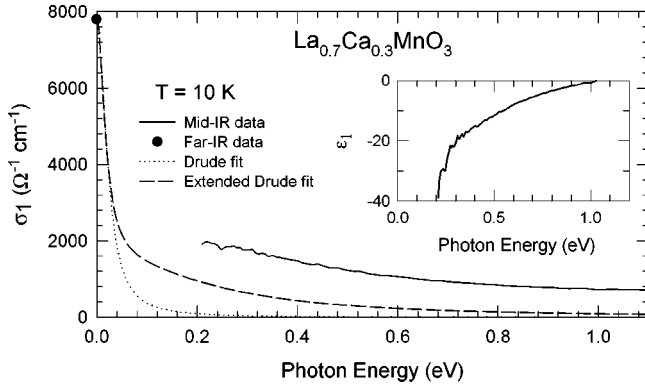


FIG. 3. Frequency dependence of the real part of the conductivity $\sigma_1(\omega)$ for LCMO. Simple and extended Drude conductivity are shown as a dotted and a dashed line, respectively. Inset shows the real part of the dielectric constant $\epsilon_1(\omega)$.

$$K(\omega) = \frac{a_0}{e^2} S(\omega) = \frac{a_0}{e^2} \frac{2}{\pi} \int_0^\omega \sigma_1(\omega') d\omega', \quad (5)$$

where a_0 is the lattice constant and $S(\omega)$ is the spectral weight. If ω is chosen to include all the optical transitions within the e_g bands K is the kinetic energy of the Mn e_g electrons. As discussed previously,² the e_g contribution to the conductivity in these materials is identified to occur in the frequency range 0–2.7 eV. The measured mid-IR conductivity for LCMO is combined with data from an earlier sample in the range 1–2.7 eV. To estimate K , a linear interpolation from the far-IR data to 0.2 eV is used (K is not sensitive to the choice of interpolation as the frequency range of the spectral gap is small). The observed K for LCMO is 280 meV, which agrees with the band theory prediction, $K_0 = 0.46t_0 \approx 280$ meV.² Considering only the contribution from the Drude conductivity, Eq. 5 gives $K_{\text{Drude}} = a_0 / (4\pi e^2) \omega_p^{*2}$. Thus, K_{Drude} from the far-IR is 28 meV, smaller than the band-structure value of 77 meV by the mass

enhancement factor $1 + \lambda$. By definition, including frequency-dependent scattering in the extended Drude model to recover the intraband spectral weight leads to the result shown as a dashed line in Fig. 3. However, as is clear from Fig. 3, the Drude conductivity alone, even including the effects of inelastic scattering, is not enough to account for the large mid-IR conductivity. Only about 1/4 of the spectral weight is predicted to be contained in the Drude term. The remaining spectral weight is most likely coming from interband transitions occurring between the two Mn e_g bands. The total infrared conductivity is then the sum of a Drude and interband contributions, $\sigma = \sigma_{\text{Drude}} + \sigma_{\text{IB}}$.

We have measured the optical properties of LCMO and LSMO thin films and obtained γ^* and m^*/m_B as a function of temperature. m^*/m_B exhibits little temperature dependence while γ^* shows a strong T^2 behavior. The optical mass enhancement differs only slightly from the specific heat mass enhancement, indicating that charge ordering correlations are not strong in these materials. Comparing the Drude weight with the measured total spectral weight, we found that the infrared conductivity is in reasonable accord with conventional contributions from both intraband and interband transitions.

Note added in proof. Since this paper was submitted a calculation of the e_g interband optical conductivity including the on site Coulomb interaction effects to lowest order in perturbation theory has come to our attention [A. Takahashi and H. Shiba, *Eur. Phys. J. B.* **5**, 413 (1998)]. The calculated optical conductivity for small $U/6t_0$ extends to $\omega = 4t_0 \approx 2.4$ eV, has a broad maximum at $\omega \approx 3t_0 \approx 2$ eV, and is otherwise relatively featureless. The experimental data reported here and in Ref. 2 is in good qualitative and semi-quantitative agreement with the calculated conductivity suggesting that the Coulomb effects are small.

We thank A. J. Millis and M. Quijada for valuable discussions. This work was supported in part by NSF-MRSEC Grants Nos. DMR-96-32521 and the NSA.

¹C. Zener, *Phys. Rev.* **82**, 403 (1951).

²M. Quijada *et al.*, *Phys. Rev. B* **58**, 16093 (1998).

³S. Kaplan *et al.*, *Phys. Rev. Lett.* **77**, 2081 (1996).

⁴S. J. L. Billinge *et al.*, *Phys. Rev. Lett.* **77**, 715 (1996).

⁵A. J. Millis, Boris I. Shraiman, and R. Mueller, *Phys. Rev. Lett.* **77**, 175 (1996); **74**, 5144 (1995); *Phys. Rev. B* **54**, 5389 (1996); **54**, 5405 (1996); H. Röder, Jun Zang, and A. R. Bishop, *Phys. Rev. Lett.* **76**, 1356 (1996).

⁶K. H. Kim, J. H. Jung, and T. W. Noh, *Phys. Rev. Lett.* **81**, 1517 (1998).

⁷Y. Okimoto *et al.*, *Phys. Rev. B* **55**, 4206 (1997).

⁸Y. Okimoto *et al.*, *Phys. Rev. Lett.* **75**, 109 (1995).

⁹H. J. Lee *et al.*, cond-mat/9904173 (unpublished).

¹⁰V. N. Smolyaninova (private communication).

¹¹J. J. Hamilton *et al.*, *Phys. Rev. B* **54**, 14926 (1996).

¹²K. Takenaka *et al.*, cond-mat/9810035 (unpublished).

¹³M. Rajeswari *et al.*, *Appl. Phys. Lett.* **71**, 2672 (1997); A. Goyal

et al., *ibid.* **71**, 2535 (1997).

¹⁴W. E. Pickett and D. J. Singh, *J. Magn. Magn. Mater.* **172**, 237 (1997).

¹⁵J. W. Allen and J. C. Mikkelsen, *Phys. Rev. B* **15**, 2952 (1977).

¹⁶P. E. Sulewski *et al.*, *Phys. Rev. B* **38**, 5338 (1988).

¹⁷R. N. Gurzhi, *Zh. Éksp. Teor. Fiz.* **35**, 965 (1958) [*Sov. Phys. JETP* **8**, 673 (1959)].

¹⁸M. Jaime, P. Lin, M. B. Salamon, and P. D. Han, *Phys. Rev. B* **58**, R5901 (1998); Kenn Kubo and Nagao Ohata, *J. Phys. Soc. Jpn.* **33**, 21 (1972).

¹⁹A. A. Abrikosov, L. P. Gorkov, and I. E. Dzyaloshinski, *Methods of Quantum Field Theory in Statistical Physics* (Dover, New York, 1975).

²⁰O. S. Heavens, *Optical Properties of Thin Solid Films* (Dover, New York, 1991), Chap. 4.

²¹F. Wooten, *Optical Properties of Solids* (Academic, New York, 1972), Chap. 6.